SIMULATION OF CARBON NANOTUBE GROWTH

BY

OGUNBUNMI, Michael Olawale

(40280)

A THESIS
SUBMITTED TO THE AFRICAN UNIVERSITY OF SCIENCE AND TECHNOLOGY
ABUJA – NIGERIA
IN PARTIAL FULFILLMENT OF THE REQUIREMENTS FOR THE AWARD OF MASTER OF SCIENCE IN THEORETICAL PHYSICS

Supervisor: Dr. Omololu Akin-Ojo

May, 2013

SIMULATION OF CARBON NANOTUBE GROWTH

A THESIS APPROVED

BY

SUPERVISOR----------
SUPERVISOR's NAME

MEMBER ----------
NAME

MEMBER----------
NAME

DEDICATION

To the Almighty God, the benevolent father whose grace has brought me this far and to my family members who through their unfeigned love and consistent prayers gave me an inner strength and enablement to crossing all hurdles. This work is humbly dedicated.

ACKNOWLEDGEMENT

If I have come this far in my academic pursuit, it is only because I had stood on the shoulders of giants. This is very true because there are many individuals who have made my MSc studies a success. I sincerely appreciate African Development Bank (ADB) for providing me with full scholarship for my studies at AUST. Special thanks goes to all the professors who had actively instructed me for this period of 18 months and particularly to Dr. Omololu Akin-Ojo who in addition made out time to supervise this work. May God richly reward each of your efforts. I also cannot fail to appreciate the Phd students who provided us with some relevant information while we were still newbie to the system, thanks to Bruno Dandogbessi, Mustapha Abdul –aguye and Kehinde Oyewole for providing me with some relevant resource materials. My fellow colleagues have also been so wonderful; they have provided me with an environment for fierce competition. The AUST communities at large have also been so wonderful in a way I cannot forget and I say thank you all for your support. I also must sincerely thank the New life Baptist Church, Suncity Abuja for the love shown to me throughout my program. May God bless you all richly in Jesus name.

Lastly but very important is the support of my parents Mr. & Mrs. Isaac Ogunbunmi who have nurtured me all through my life and provided me with a strong financial base. How can I thank you enough for all you've done for me and to my dear friend Adeola Akinsola who I can comfortably share my challenges and visions with. In your friendship I have found comfort. To the only wise God immortal, invisible God only wise be glory honor and adoration now and forever Amen.

ABSTRACT

The basic understanding of the underlying techniques of growing Carbon Nanotubes (CNTs) with a specific chirality is still obscure and needs to be understood so as to properly harness its potentials. Using both Classical Molecular Dynamics (MD) simulation with empirical force fields and a geometry optimization based on ab initio forces, we show that the dynamics involved in the growth of CNT on iron nanoparicles is non linear but complex. For a good geometry, the growth depends on the deposition rate of the carbon atoms on the iron nanoparticles. Observations show that defects in the CNT first appear in the cap formed and then propagate through the wall of the growing tube. Partial results from ab initio show the formation of a cap which is a precursor of an armchair type CNT.

TABLE OF CONTENTS

CHAPTER ONE

1.0.0 INTRODUCTION

Carbon nanotubes (CNT) occur as allotropes of carbon, others being diamond, graphite and fullerenes. Their walls are formed by an atom thick sheet of graphite(called graphene) rolled into cylinders[1]. The diameters are in the order of nanometer and the length in micrometers. In recent times, nanotubes of length-to-diameter ratio of 132,000,000:1 have been constructed. This big ratio leads to a huge and unusual electrical transport. The bonds present are sp^2 which is much similar to those of graphite[2] and the tubes align themselves together by a van der Waals forces (pi-stacking).

When the graphite sheets are rolled up in a discrete(chiral) angle and a given radius with respect to a plane perpendicular to the tubes long axis, a CNT of specific chirality (either metallic or semiconducting) is formed depending on the combination of the rolling angle and the radius[3].

(a) (b) (c)

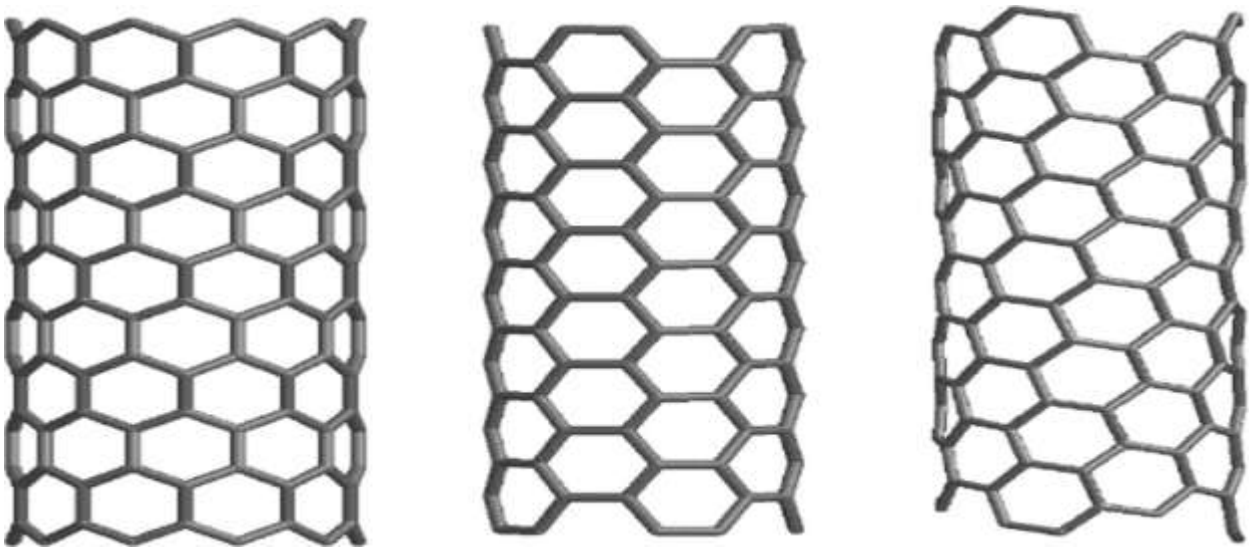

Fig.1.1. The outlines of three types of nanotube: (a) a (10,0) zigzag nanotube; (b) a (5,5) armchair nanotube; (c) a (7,3) general chiral nanotube.(Rafil, 2008)

The angle usually can range from 0-30^o[5]. This rolling up of the graphene sheet is represented by a pair of indices (n_1,n_2) where n_1 and n_2 denotes the number of unit vectors along the direction of the honey comb crystal lattice of graphene [4].For n_2 =0 the nanotube is said to be zigzag with chiral angle=0, for n_1=n_2 it is armchair with chiral angle=30^o, otherwise it is chiral. One can also show [18] that the bandgap of the CNT is a function of |n2 - n1| and, hence, the indices (n_1,n_2) determine whether the CNT is metallic or semiconducting.

Their discovery by Sumio Lijima of NEC in 1991[5]has come to be a giant leap in Science and Technology and has since then been envisioned as a step to revolutionalizing nanotechnology. This is true considering their many unique properties ranging from being 100 times stronger than stainless steel and six times lighter, hard as diamond but thermal capacity twice that of pure diamond, current-carrying capacity of 1000 times higher than that of copper, and thermally stable up to 4000K[8].

Their wide range of applications are also astonishing in the sense that it opens the possibility of weaving them into clothes that are bullet proof and stab-proof, further miniaturization of electronic devices, production of paper batteries, production of solar cells of improved efficiencies, treatment of cancerous cells e.t.c.

So far, there have been many growth techniques employed in the production of nanotubes. They include laser ablation, arc discharge, high pressure carbon monoxide disproportionate (Hipco) and chemical vapor deposition (CVD)[8]. Of all these, CVD approach has proven more promising for large scale production, and the ease to directly grow the CNT on any given substrate [8].

The CVD approach involves using a substrate containing particles of metallic catalyst usually cobalt, iron, nickel or their combination[6].

There are diverse opinions about the mechanism of CNT growth, but the most accepted one is described by Kumar [8]. A hydrocarbon is passed through a chamber containing transition metal nanoparticles at a very high temperature. Meyyapan reported that CNT growth does not occur below 550 degree Celsius [5]. The hydrocarbon (usually methane) is broken down and a carbon deposit is created while the hydrogen escapes[7]. The carbon deposit diffuses into the metal nanoparticles catalyst. It nucleates within it and latter precipitates out a cylindrical network with no dangling bond and energetically stable. This is the CNT and in other instances gives carbon nanofibres (CNFs). The process is sustained due to the thermal gradient inside the metal nanoparticles. There are two modes of growth namely, base growth (when the metallic catalyst is lifted by the growing carbon nanostructures) and tip growth (when the metallic catalyst remains at the bottom of the CNT), these he said depends on the energy gained as a result of adding carbon atoms from the carbon metal catalyst solution to the graphene sheets forming the carbon nanostructures [7]. However, Kumar reported that when the catalyst-substrate interaction is weak, the carbon diffuses down through the metal; the CNT precipitates out at the metal bottom thereby pushing the metal catalyst off the substrate. The growth continues as long as the metal's top is open for carbon diffusion but stops when the surface is completely covered with the excess carbon which stops the catalytic activities. When the catalyst-substrate interaction is strong, carbon diffuses into the metal catalyst, but this time the CNT precipitation fails to push the metal particles up so that the CNT emerge out from the metal apex.

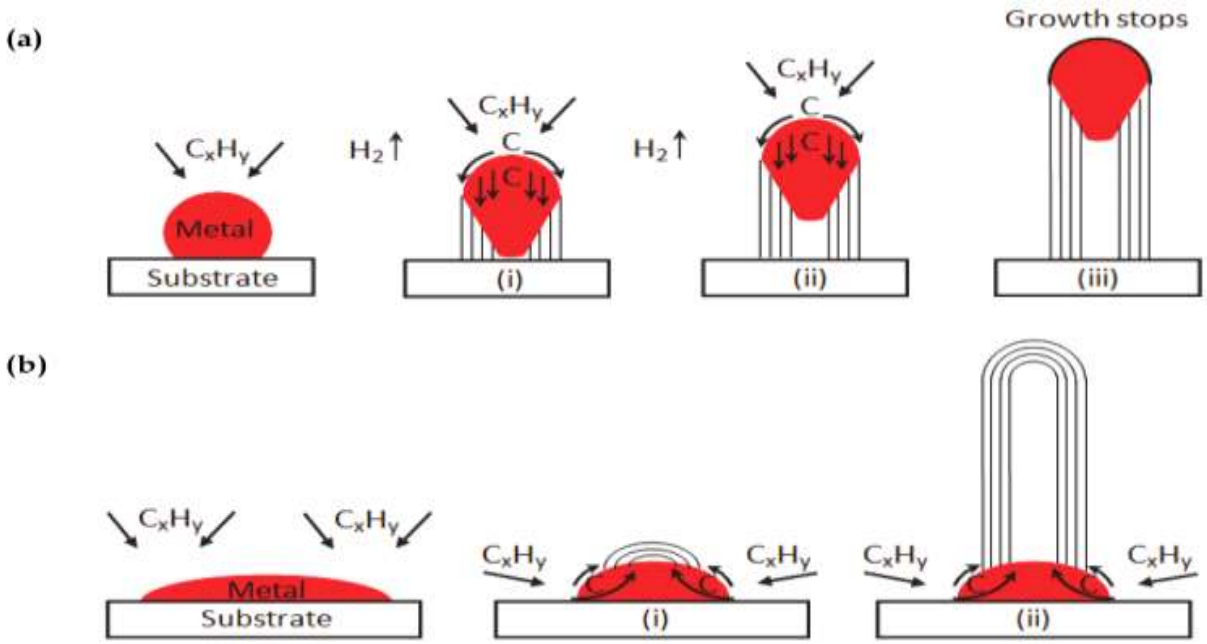

Fig1.2. Widely-accepted growth mechanisms for CNTs: (a) tip-growth model, (b) base- growth model (Banerjee etal,2008)

Despite the huge advancement made so far in the production of CNT, yet there is no known mechanism for controlling the chirality of CNT during the growth process whether it will be semiconducting or metallic[3]. Factors or parameters that influence a specific growth still needed to be understood. Is the mechanism sensitive to metal catalyst, catalyst size, carbon precursor, the substrate type, temperature, pressure e.t.c? These and many more are questions awaiting answers about CNT growth.

Stephanie *et. al.* [3] proposed an idea for the chirality-selective growth of nanotubes by controlling the type of caps that form on the catalyst at the nucleation stage by ab-initio calculation. The work of Raty *et. al.* [2] (see fig2) further demonstrated convincingly the possibility of achieving the growth mechanism by ab- initio simulation.

It is therefore in the interest of this work to attempt answering some of the questions above through both classical Molecular Dynamics (MD) and ab-initio simulation similar to that of Raty *et. al.* but by employing other necessary means to understand the nanotube growth mechanism.

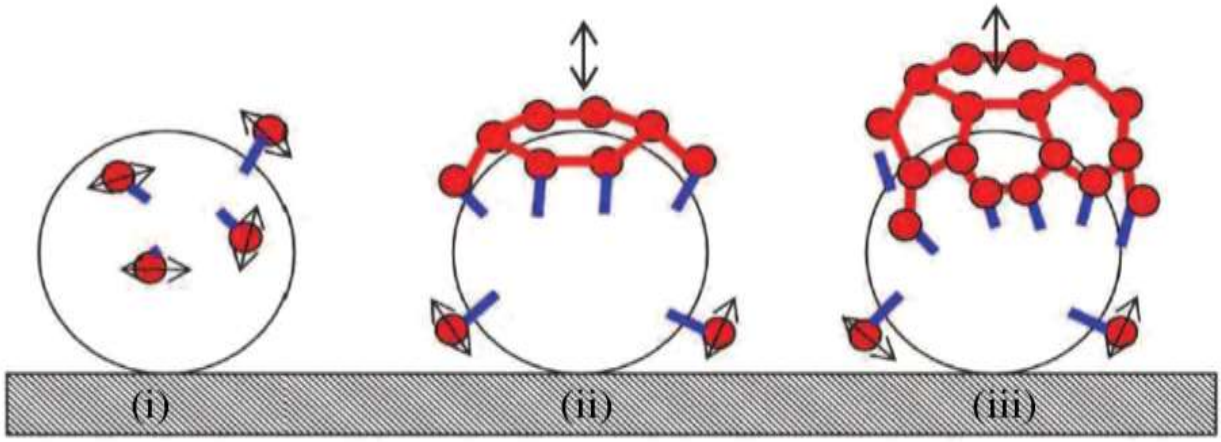

Fig1.3. Schematic representation of the basic steps of SWCNT growth on a Fe catalyst, as observed in ab initio simulations. (I) Diffusion of single C atoms (red spheres) on the surface of the catalyst. (ii) Formation of a sp^2 graphene sheet floating on the catalyst surface with edge atoms covalently bonded to the metal. (iii) Root incorporation of diffusing single C atoms.[Raty *et. al.*, 2005]

1.1.0 AIMS AND OBJECTIVES

The aim of this work is to understand the mechanism by which certain chirality occur in carbon nanotube growth processes.

The objectives are

1) Perform molecular dynamics simulation using empirical force fields (with LAMMPS codes) of carbon on nanoparticles of Fe
2) Carry out Born-Oppeinheimer MD simulations and geometry optimization of carbon atoms on iron nanoclusters. Here, the program used will be Quantum Espresso.

CHAPTER TWO

2.0.0 THEORY

2.1.0 Geometry of a Graphene Sheet

The geometry of a graphene sheet (i.e. atom thick graphite) is crucial to a good understanding of the various properties of Carbon Nanotube (CNT). Consider the graphene sheet as shown below

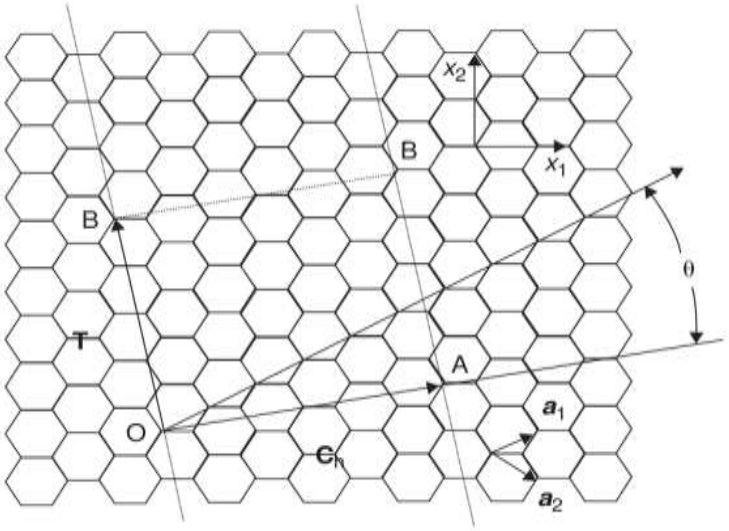

Fig2.1. A 2-D graphene sheet showing the vectors that characterize SWCNT (Drasselhaus *et. al.*)

Where the x_1 and x_2-axes are respectively parallel to a so-called armchair direction and a zigzag direction of the sheet. The point O is the origin in the sheet. Any other equivalent point, such as A, can be reached by the use of the Bravais lattice vector $\mathbf{C}_h$ of the graphene sheet. The vectors $\mathbf{a}_1$ and $\mathbf{a}_2$ are the primitive vectors of the unit cell. The vector **T** is another lattice vector, which is normal to the vector $\mathbf{C}_h$, connecting the two equivalent points O and B. The vector $\mathbf{C}_h$ is referred to as the chiral vector and the angle θ that it makes with the zigzag axis of the graphene sheet passing through O is called the chiral angle.

In Cartesian coordinates the primitive vectors are given as

$$\mathbf{a_1} = a\left(\frac{\sqrt{3}}{2}\widehat{\mathbf{e}_1} + \frac{1}{2}\widehat{\mathbf{e}_2}\right),$$

$$\mathbf{a_2} = a\left(\frac{\sqrt{3}}{2}\widehat{\mathbf{e}_1} - \frac{1}{2}\widehat{\mathbf{e}_2}\right) \text{----------2.1}$$

Where $\widehat{\mathbf{e}_1}$ and $\widehat{\mathbf{e}_2}$ are unit vectors along the x_1- and x_2-axes, respectively, and a = 2.46 Ang. is the lattice constant of graphite. This constant is related to the carbon–carbon bond length a_{C-C} by

$$a = \sqrt{3}aC - C \text{----------2.2}$$

The area of the unit cell for the basis vectors shown in Figure 2.1 is given by

$$S_G = |\mathbf{a}_1 \times \mathbf{a}_2| = \frac{\sqrt{3}a^2}{2} \text{----------2.3}$$

The chiral vector is obtained from the basis vectors as

$$\mathbf{C}_h = n\mathbf{a_1} + m\mathbf{a_2} \text{----------2.4}$$

Putting (2.1) into (2.4) gives

$$\mathbf{C}_h = \frac{\sqrt{3}a}{2}(n+m)\widehat{\mathbf{e}_1} + \frac{a}{2}(n-m)\widehat{\mathbf{e}_2} \text{----------2.5}$$

Where (n, m) are a pair of integers that characterize the chiral vector, and are referred to as the chiral indices. The length L of the chiral vector is given as

$$L = |\mathbf{C}_h| = a(n^2 + m^2 + nm)^{\frac{1}{2}} \text{ ----------2.6}$$

The chiral angle, as depicted in Figure 2.1, can be obtained from

$$\cos\theta = \frac{\mathbf{a_1}.\mathbf{C}_h}{|\mathbf{a_1}||\mathbf{C}_h|} \text{ ----------2.7}$$

Or, by using (2.1) and (2.5),

$$\cos\theta = \frac{2n+m}{2(n^2 + m^2 + nm)^{\frac{1}{2}}} \text{ ----------2.8}$$

So that

$$\sin\theta = \frac{\sqrt{3}m}{2(n^2 + m^2 + nm)^{\frac{1}{2}}},$$

$$\tan\theta = \frac{\sqrt{3}m}{2n+m}. \text{ ----------2.9}$$

2.2.0 Geometry of an SWCNT

Rolling the sheet shown in Figure 2.1 so that the end of the chiral vector $\mathbf{C}_h$, i.e. the lattice point A, coincides with the origin O leads to the formation of an (n,m) nanotube whose circumference is the length of the chiral vector, and whose diameter d_t is therefore

$$d_t = \frac{L}{\pi} = \frac{a(n^2 + m^2 + nm)^{\frac{1}{2}}}{\pi} \text{ ----------2.10}$$

Since the zigzag axis of the sheet corresponds to θ = 0, then if the rolling chiral vector is along this axis, a zigzag SWCNT is generated. From (2.11), we see that θ = 0 corresponds to m = 0,

and hence a zigzag SWCNT is an (n, 0) nanotube. On the other hand, the armchair axis of the sheet is specified by $\theta = \pi/6$, and if this is the direction of the rolling chiral vector, an armchair nanotube is generated. Again from (2.10) we see that $\theta = \pi/6$ corresponds to m = n, and hence an armchair SWCNT is an (n, n) nanotube. An SWCNT generated for any other value of θ, i.e. $0<\theta<\pi/6$, is referred to as a general chiral SWCNT. Figure 2.2 shows the schematic representations of these three types of nanotube.

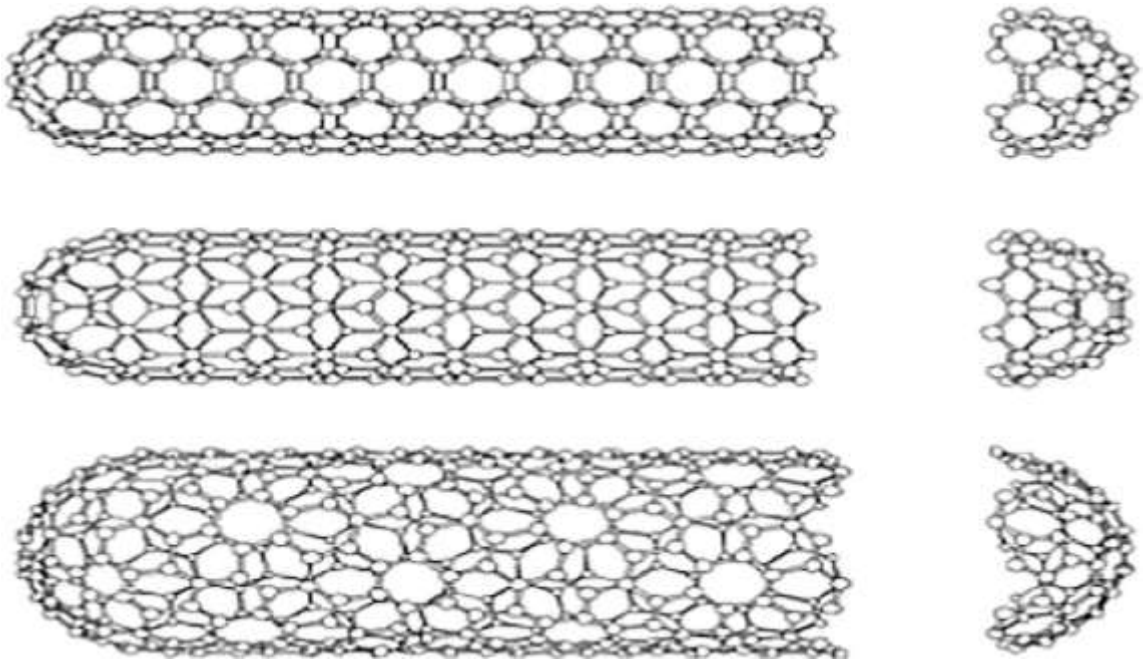

Fig. 2.2 Models of capped SWCNTs, showing: (a) a (5,5) armchair nanotube; (b) a zigzag (9,0) nanotube; (c) a general chiral (10,5) nanotube. (Drasselhaus *et. al.*)

Therefore, each real lattice vector $\mathbf{C}_h$ defines a different way of rolling up the sheet into an SWCNT. The point-group symmetry of the lattice makes many of these nanotubes equivalent. So the unique SWCNTs are generated by using only a 1/12 irreducible wedge of the Bravais lattice, i.e. the wedge contained between $\theta = 0$ and $\theta = \pi/6$. The unit cell of an SWCNT, shown in Figure 2.1, is the rectangle OAB'B bounded by the vectors $\mathbf{C}_h$ and **T**. We need to derive an expression

for **T** in terms of the unit vectors $\mathbf{a}_1$ and $\mathbf{a}_2$, and the indices (n,m) that are used to construct the vector $\mathbf{C}_h$. To do so, let us first write the unit vector along $\mathbf{C}_h$ on the basis of (2.5):

$$\widehat{\mathbf{C}_h} = \frac{\sqrt{3}a}{3L}(n+m)\widehat{\mathbf{e_1}} + \frac{a}{2L}(n-m)\widehat{\mathbf{e_2}} \quad \text{----------2.11}$$

The unit vector, along the vector T, perpendicular to $\widehat{\mathbf{C}_h}$ can be written as

$$\hat{\mathbf{T}} = \alpha\widehat{\mathbf{e_1}} + \beta\widehat{\mathbf{e_2}}. \quad \text{----------2.12}$$

Then from the condition

$$\widehat{\mathbf{C}_h} \cdot \hat{\mathbf{T}} = 0, \quad \text{----------2.13}$$

and the fact that the lengths of the two unit vectors $\widehat{\mathbf{C}_h}$ and $\hat{\mathbf{T}}$ are equal, we obtain

the following equations:

$$\frac{\sqrt{3}a}{2L}(n+m) + \beta\frac{a}{2L}(n-m) = 0,$$

$$\frac{3a^2}{4L^2}(n+m)^2 + \frac{a^2}{4L^2}(n-m)^2 = \alpha^2 + \beta^2. \quad \text{----------2.14}$$

Solving these two equations gives

$$\alpha = \frac{-a}{2L}(n-m),$$

$$\beta = \frac{\sqrt{3}a}{2L}(n+m), \quad \text{----------2.15}$$

And hence from (2.14)

$$\hat{\mathbf{T}} = \frac{a}{2L}\left[-(n-m)\widehat{\mathbf{e_1}} + \sqrt{3}(n+m)\widehat{\mathbf{e_2}}\right], \text{----------2.16}$$

And the vector **T** is given by

$$\mathbf{T} = |\mathbf{T}|\hat{\mathbf{T}}. \text{----------2.17}$$

We can express the magnitude of **T** as a proportion of the magnitude of vector $\mathbf{C}_{h:}$

$$|\mathbf{T}| = \eta L, \text{----------2.18}$$

Where η is the proportionality constant. Substituting from (2.16) and (2.18) into into (2.17), we have

$$\mathbf{T} = \eta\frac{a}{2}\left[-(n-m)\widehat{\mathbf{e_1}} + \sqrt{3}(n+m)\widehat{\mathbf{e_2}}\right] \text{----------2.19}$$

On the other hand, since **T** is a chiral vector, we can write

$$\mathbf{T} = t_1\mathbf{a_1} + t_2\mathbf{a_2} \text{----------2.20}$$

Where (t_1, t_2) are a pair of integers. Comparison of (2.19) and (2.20) gives

$$t_1 = \frac{\eta(n+2m)}{\sqrt{3}},$$

$$t_2 = \frac{-\eta(2n+m)}{\sqrt{3}}. \text{----------2.21}$$

To determine the constant η, we should remember that, as we have said before, the

Vector **T** connects the origin O to the first equivalent lattice point B. This implies that

the integers t_1 and t_2 cannot have a common divisor, save for unity. In consequence,

$$\frac{\eta}{\sqrt{3}} = \frac{1}{d_{\mathbf{R}}} \text{ ----------2.22}$$

Where

$$d_{\mathbf{R}} = hcd(n+2m, 2n+m), \text{ ----------2.23}$$

and hcd stands for the highest common divisor. Therefore,

$$t_1 = \frac{(n+2m)}{d_{\mathbf{R}}},$$

$$t_2 = \frac{-(n+2m)}{d_{\mathbf{R}}}. \text{ ----------2.24}$$

If

$$d = hcd(n,m), \text{ ----------2.25}$$

then

$$d_{\mathbf{R}} = \left\{ \begin{array}{l} \text{d if } (\text{n} - \text{m}) \text{ is not a multiple of 3d,} \\ \text{3d if } (\text{n} - \text{m}) \text{ is a multiple of 3d.} \end{array} \right\} \text{----------2.26}$$

Substituting for η from (2.22) into (2.18), we obtain the length of the vector **T** as

$$|\mathbf{T}| = \eta L = \frac{\sqrt{3}L}{d_{\mathbf{R}}}. \quad \text{----------2.27}$$

For example, if we consider the chiral vector

$$\mathbf{C}_h = 17\mathbf{a_1} + 5\mathbf{a_2}. \quad \text{----------2.28}$$

in the Cartesian coordinate system, the basis vectors are given by in this case by d = 1, and, since the second condition in (2.26) holds, then $d_{\mathbf{R}} = 3$, and hence, from (2.20) and (2.24) the vector **T** is given by

$$\mathbf{T} = 9\mathbf{a_1} + 13\mathbf{a_2}. \quad \text{----------2.29}$$

To compute the number of atoms per unit cell of the SWCNT, we need to divide the area of the SWCNT unit cell $\mathbf{S_T}$ by the area of the graphene unit cell $\mathbf{S_G}$ given in (2.13). The area of the SWCNT unit cell is given by

$$S_T = |T||\mathbf{C}_h| = \frac{\sqrt{3}L}{d_R}L, \quad \text{----------2.30}$$

or employing (2.8)

$$S_T = \frac{\sqrt{3}a^2(n^2 + m^2 + nm)}{d_{\mathbf{R}}}. \quad \text{----------2.31}$$

Therefore, the number of atoms N_T per unit cell of the SWCNT is given by

$$N_T = 2\frac{S_T}{S_G} = \frac{4(n^2 + m^2 + nm)}{d_R}, \quad \text{----------2.32}$$

Where the factor two is included to account for the two atoms per unit cell of the graphene sheet. The expressions for the geometry of an SWCNT derived above assume, implicitly, that the act of rolling the graphene sheet into a cylindrical nanotube does not significantly distort the relative distance of the two carbon atoms within the hexagonal shells. This means that the carbon–carbon bond length on the surface of the nanotube is still a_{C-C}, introduced in (2.11).

The graphene sheet is a semi metallic material with a zero band gap. The electronic states of an infinitely long SWCNT are continuous in the axial direction of the nanotube, but are quantized in the circumferential direction. The electronic properties of these nanotubes are determined by their (n,m) chiral indices according to the rules[18]

$$if\ \frac{(n-m)}{3}\begin{cases} = \text{integer, then the nanotube is metallic} \\ \neq \text{integer, then the nanotube is semiconducting} \end{cases} \text{----------2.33}$$

The armchair SWCNT is, therefore, always metallic, and, for a semiconducting SWCNT of diameter d_t, the bandgap scales as $1/d_t$ [1,18].However, the breaking of the bond symmetry due to curvature can give rise to the appearance of a small band-gap even in the metallic SWCNTs, hence turning them into small-gap semiconducting materials.[1]

2.3.0 Classical Molecular Dynamics (MD) Simulation Method

An MD simulation is often carried out on a model nano sized system composed of N interacting atoms, or molecules. The interactions, described by appropriate interatomic potentials, can be of either a pair-wise, or many-body, type. These potentials characterize the physics of the nano systems, which can be in any phase, i.e. solid, liquid or gas. One of the objectives of MD simulations is to obtain the properties of the nano system as time-averages of the instantaneous properties when the constituent atoms move in the course of the simulation time, and the nano system switches from one state to another state. Given the initial position coordinates and velocities of the atoms in the nano system, the subsequent motion of

individual atoms is described either by deterministic Newtonian dynamics or by Langevin type stochastic dynamics, depending on the type of system we are dealing with. In a classical MD simulation, the model nano system is confined to a simulation cell of volume V. This cell, called the central simulation cell, is then typically replicated in all spatial dimensions, corresponding to the dimensionality of the system. This replication generates the periodic images of the cell, as well as the periodic images of the original N atoms within this cell, giving rise to the so- called the periodic boundary condition (PBC). The imposition of the PBC is necessary to compensate for the unwanted effects of the artificial surfaces that accompany a model system with a finite size, when computation of the bulk properties is required. For example, for a system composed of 1000 molecules located in a 10 × 10 × 10 cubic simulation cell, about 488 molecules are located on the faces of the cell, and these molecules experience different forces from those in the interior of the cell. In the course of an MD simulation, the atoms in the original model system, placed in the central simulation cell, move in this cell, and correspondingly their periodic images execute an exactly identical motion in their respective image cells. When one atom leaves the central cell from one side, one of its periodic images enters from the opposite side, via the implementation of the PBC. This keeps the number of atoms in the central cell constant.

2.3.1 Computation of forces

This computation is by far the most important, and time-consuming, part of MD code. If the energetics of the atoms are described by a potential energy function $H_I(r_{ij})$ then, in a Newtonian dynamics-based simulation, the force experienced by each atom at each simulation time-step is computed from this potential according to

$$\mathbf{F}_i = -\sum_{j>i} \nabla_{\mathbf{r}i} H_I(r_{ij}), \quad \text{----------2.34}$$

where r_{ij} is the separation distance between two atoms i and j. If the potential energy function is described by a two-body interaction function, then a particular atom in the simulation cell interacts with N − 1 atoms in the same cell, as well as with the periodic images of these atoms

located in the image cells. This amounts to a prohibitively large number of interactions and computational time. When the inter atomic potential is short-ranged then, in order to save computing time, the simplifying assumption is often made, in the module that computes the forces, that each atom in the simulation cell interacts only with the nearest periodic images of the N −1 neighbors. This involves the computation of [N (N − 1)]/2 interactions. This assumption, named the minimum-image convention , is implemented in practice by imagining the particular atom under consideration to be located at the centre of a box, of the same shape and size as the central simulation cell, and interacting with all the atoms that fall within this box, i.e. with the nearest periodic images of the remaining N − 1 atoms. Further simplification involves imposing a cut-off distance on these neighbors of the atom and considering only those neighbors, from among the reduced number of neighbors, that are located within a specified cut-off sphere within this imaginary box whose centre coincides with that of the box. For a cubic central simulation cell, the radius of this cut-off sphere must not be greater than half the length of the simulation cell. To find the neighbors of the atoms, a module that creates a list of neighbors of the atoms is called after every few time-steps.

2.3.2 Equations of Motion

Once the forces experienced by individual atoms are computed, the motion of the N atoms is obtained by integrating 3N simultaneous coupled Newton's equations of motion. These equations can be integrated numerically by a variety of algorithms. These algorithms are based on the finite-difference method, wherein the time-variable is discretized on a finite grid. Knowledge of the position $r_i(t)$, velocity $v_i(t)$ and force $F_i(t)$ experienced by the atom i at simulation time t allows the integration scheme to compute the same quantities at a later time (t+dt).Among the many integration schemes that are available, one very popular algorithm is the

velocity Verl*et al*gorithm. According to this algorithm, the positions r_i and velocities v_i of the atoms of mass m_i are updated after each simulation time-step dt by

$$\mathbf{r}_i(t+dt) = \mathbf{r}_i(t) + \mathbf{v}_i(t) + \frac{1}{2}(dt)^2 \frac{\mathbf{F}_i(t)}{m_i}, \quad \text{----------2.35}$$

$$\mathbf{v}_i\left(t+\frac{1}{2}dt\right) = \mathbf{v}_i(t) + \frac{1}{2}dt\frac{\mathbf{F}_i(t)}{m_i},$$

$$\mathbf{v}_i(t+dt) = \mathbf{v}_i\left(t+\frac{1}{2}dt\right) + \frac{1}{2}dt\frac{\mathbf{F}_i(t+dt)}{m_i}, \quad \text{----------2.36}$$

where the choice of the size of dt depends on several factors, such as the temperature, density and masses of the atoms involved and the nature of the force law . Once the velocities are computed, the instantaneous kinetic energies, and hence the instantaneous temperature and the instantaneous pressure can be computed. Such data on the instantaneous values allow for the computation of time-averaged values at the conclusion of the simulation.

2.4.0 Ab-initio molecular dynamics simulation methods

In classical MD simulation method the forces experienced by the atoms in many-body nanoscale systems are obtained from prescribed interatomic potential energy functions, and these potentials express the basic physics of the model system at hand. In this approach, access to pertinent potential energy functions is crucial. Such functions can be constructed either as pair-potentials, or as cluster expansions involving pair-potentials, plus three-body and many body potentials, or they can be expressed as functionals of pair-potentials[1].

Alternative, quantum-mechanical-based methods that are free from interaction potentials have been developed, and these are referred to as ab initio molecular dynamics simulation methods. The essence of an ab initio method consists of deriving the forces experienced by the atomic

nuclei in a nanosystem, not from predefined interatomic potentials fixed in advance, but from electronic structure calculations as the simulation is progressing and the particle trajectories are evolving in the phase space of the system. Therefore, the electronic degrees of freedom become explicitly relevant to the understanding of the behavior of the nanosystem. Consequently, when the ab initio MD methods are used, the priority is shifted from the construction of approximate potential energy functions beforehand, to the choice of the approximate schemes for computing the many-body Schrödinger equation. The advantage of these ab initio methods lies in the fact that many scenarios unforeseen before the start of the simulation are allowed to develop during the course of the simulation.

In non relativistic quantum mechanics, the energy level of a system composed of N nuclei located at positions

$\{\mathbf{R}_I\} \equiv \{\mathbf{R}_1, \mathbf{R}_2, \ldots, \mathbf{R}_N\}$,----------2.37

with momenta

$\{\mathbf{P}_I\} \equiv \{\mathbf{P}_1, \mathbf{P}_2, \ldots, \mathbf{P}_N\}$,----------2.38

and N_e electrons located at positions

$\{\mathbf{r}_i\} \equiv \{\mathbf{r}_1, \mathbf{r}_2, \ldots, \mathbf{r}_{Ne}\}$,----------2.39

with momenta

$\{\mathbf{p}_i\} \equiv \{\mathbf{p}_1, \mathbf{p}_2, \ldots, \mathbf{p}_{Ne}\}$,----------2.40

and spin variables

$\{\mathbf{s}_i\} \equiv \{\mathbf{s}_1, \mathbf{s}_2, \ldots, \mathbf{s}_{Ne}\}$,----------2.41

are obtained from the independent Schrodinger equation

$H\Psi(\{\mathbf{X}_i\},\{\mathbf{R}_I\}) = E(\{\mathbf{X}_i\},\{\mathbf{R}_I\})$, ----------2.42

Where

$\{\mathbf{x}_i\} \equiv (\{\mathbf{r}_i\}, \{\mathbf{s}_i\})$,----------2.43

denotes the set of position and spin variables. The corresponding total Hamiltonian is given by

$$H^{tot} = \sum_{I=1}^{N} \frac{\mathbf{P}_I^2}{2M_I} + \sum_{I}^{N_e} \frac{\mathbf{P}_i^2}{2m} + \sum_{i>j} \frac{e^2}{|\mathbf{r}_i - \mathbf{r}_j|} + \sum_{i>j} \frac{Z_I Z_J e^2}{|\mathbf{R}_I - \mathbf{R}_J|} - \sum_{i,I} \frac{Z_I e^2}{|\mathbf{R}_I - \mathbf{r}_i} = K_N + K_e + H_I^{ee}(\{\mathbf{r}_i\}) + H_I^{NN}(\{R_I\}) + H_I^{eN}(\{\mathbf{r}_i\}, \{\mathbf{R}_I\}),$$

----------2.44

where m and M_I are respectively the masses of the electron and the Ith nucleus, $Z_I e$ is the charge on the Ith nucleus, K_N, K_e, H_I^{ee}, H_I^{NN} and H_I^{eN} are, respectively, the operators representing the nuclear kinetic energy, the electron kinetic energy, the electron–electron interaction, the nucleus–nucleus interaction and the electron– nucleus interaction. The Schrödinger equation (2.42) is therefore written as

$$[K_N + K_e + H_I^{ee}(\{\mathbf{r}_i\}) + H_I^{NN}(\{\mathbf{R}_I\}) + H_I^{eN}(\{\mathbf{r}_i\}, \{\mathbf{R}_I\})]\Psi(\{\mathbf{X}_i\}, \{\mathbf{R}_I\}) = E\Psi(\{\mathbf{X}_i\}, \{\mathbf{R}_I\}).$$ ------2.45

We look for the eigenfunctions and eigenvalues of (2.45). While obtaining an exact solution of (2.45), even for simple molecules, is impractical, an approximation scheme, called the Born–Oppenheimer approximation (BOA), can be invoked to obtain an approximate solution. The BOA is based on separating the fast and slow motions present in the system, i.e. separating the nuclear and electronic motions, because of the large disparity that exists between the nuclear and electronic masses. To implement the BOA scheme, the total wave function is expressed as the product ansatz

$$\Psi(\{\mathbf{X}_i\}, \{\mathbf{R}_I\}) = \phi^{eI}(\{\mathbf{X}_i\}, \{\mathbf{R}_I\})\phi^{nuc}(\{\mathbf{R}_I\}),$$ ----------2.46

where $\phi^{nuc}(\{\mathbf{R}_I\})$ is the nuclear wave function, and $\phi^{eI}(\{\mathbf{X}_i\}, \{\mathbf{R}_I\})$ is the electronic wave function, whose dependence on nuclear positions is parametric.

Operating K_N on (2.46) gives

$$K_N\phi^{el}(\{\mathbf{X}_i\},\{\mathbf{R}_I\})\phi^{nuc}(\{\mathbf{R}_I\}) = \frac{\hbar^2}{2}\left(\sum_{I=1}^{N}\frac{1}{M_I}[\phi^{el}(\{\mathbf{X}_i\},\{\mathbf{R}_I\})\nabla_I^2\phi^{nuc}(\{\mathbf{R}_I\}) + \phi^{nuc}(\{\mathbf{R}_I\})\nabla_I^2\phi^{el}(\{\mathbf{X}_i\},\{\mathbf{R}_I\}) \right.$$
$$\left. +2\nabla I\phi^{el}(\{\mathbf{X}_i\},\{\mathbf{R}_I\})\cdot\nabla I\phi^{nuc}(\{\mathbf{R}_I\})]\right).$$

----------2.47

The use of the BOA implies neglecting the terms $\nabla I\phi^{el}(\{\mathbf{X}_i\},\{\mathbf{R}_I\})$, since the nuclear

wavefunction is more localized than the electronic wavefunction , and hence it is expected that

$$\nabla I\phi^{nuc}(\{\mathbf{R}_I\}) \gg \nabla I\phi^{el}(\{\mathbf{X}_i\},\{\mathbf{R}_I\})$$ ----------2.48

Substitution of (2.46) into (2.45) and invoking the BOA leads to

$$[K_e + H_I^{ee}(\{\mathbf{r}_i\}) + H_I^{eN}(\{\mathbf{r}_i\},\{\mathbf{R}_I\})]\phi^{el}(\{\mathbf{X}_i\},\{\mathbf{R}_I\})\phi^{nuc}(\{\mathbf{R}_I\}) + \phi^{el}(\{\mathbf{X}_i\},\{\mathbf{R}_I\})K_N\phi^{nuc}(\{\mathbf{R}_I\}) +$$ -----
$$H_I^{NN}(\{\mathbf{R}_I\})\phi^{el}(\{\mathbf{X}_i\},\{\mathbf{R}_I\})\phi^{nuc}(\{\mathbf{R}_I\}) = E\phi^{el}(\{\mathbf{X}_i\},\{\mathbf{R}_I\})\phi^{nuc}(\{\mathbf{R}_I\}).$$

----------2.49

Dividing both sides of (3.162) by $\phi^{el}(\{\mathbf{X}_i\},\{\mathbf{R}_I\})\phi^{nuc}(\{\mathbf{R}_I\})$,

$$\frac{[K_e + H_I^{ee}(\{\mathbf{r}_i\}) + H_I^{eN}(\{\mathbf{r}_i\},\{\mathbf{R}_I\})]\phi^{el}(\{\mathbf{X}_i\},\{\mathbf{R}_I\})}{\phi^{el}(\{\mathbf{X}_i\},\{\mathbf{R}_I\})} = E - \frac{[K_N + H_I^{NN}(\{\mathbf{R}_I\})\phi^{nuc}(\{\mathbf{R}_I\})}{\phi^{nuc}(\{\mathbf{R}_I\})}$$ ---------2.50

An examination of (2.50) shows that its right-hand side is a function of $\{R_I\}$ alone, and if this

dependence is expressed by a function $f(\{R_I\})$, i.e.

$$\frac{[K_e + H_I^{ee}(\{\mathbf{r}_i\}) + H_I^{eN}(\{\mathbf{r}_i\},\{\mathbf{R}_I\})]\phi^{el}(\{\mathbf{X}_i\},\{\mathbf{R}_I\})}{\phi^{el}(\{\mathbf{X}_i\},\{\mathbf{R}_I\})} = f(\{\mathbf{R}_I\})$$ ----------2.51

then (2.50) can be written as

$$[K_e + H_I^{ee}(\{\mathbf{r}_i\}) + H_I^{eN}(\{\mathbf{r}_i\},\{\mathbf{R}_I\})]\phi^{el}(\{\mathbf{X}_i\},\{\mathbf{R}_I\}) = f(\{\mathbf{R}_I\})\phi^{el}(\{\mathbf{X}_i\},\{\mathbf{R}_I\})$$ ----------2.52

This is an eigenvalue equation from which the Hamiltonian for electrons can be read:

$$H^{el}(\{\mathbf{R}_I\}) = K_e + H_I^{ee}(\{\mathbf{r}_i\}) + H_I^{eN}(\{\mathbf{r}_i\},\{\mathbf{R}_I\}).$$ ----------2.53

The dependence of the associated sets of eigenfunctions and eigenvalues,

$\phi_n^{el}(\{\mathbf{X}_i\},\{\mathbf{R}_I\})$ and $f_n(\mathbf{R}_I\})$ respectively, on $\{\mathbf{R}_I\}$ is parametric.

Corresponding to every solution of (2.53), there is an associated nuclear eigenvalue equation

$$[K_N + H_I^{NN}(\{\mathbf{R}_I\}) + f_n(\mathbf{R}_I\})]E\phi^{nuc}(\{\mathbf{R}_I\}). \text{ ----------2.54}$$

Furthermore, the nuclear dynamics unfold on an electronic surface which is generated by every eigenvalue $f_n(\{R_I\})$ of the electronic eigenvalue equation (2.52). The nuclear dynamics follow the time dependent Schrödinger equation

$$[K_N + H_I^{NN}(\{\mathbf{R}_I\}) + f_n(\mathbf{R}_I\})]\phi^{nuc}(\{\mathbf{R}_I\},t) = i\hbar\frac{\partial}{\partial t}\phi^{nuc}(\{\mathbf{R}_I\},t) \text{ ----------2.55}$$

where $\phi^{nuc}(\{\mathbf{R}_I\},t)$ is the time-dependent nuclear wavefunction. The implication of (2.55) is that the electrons respond instantaneously to the nuclear motion and, therefore, for each configuration $\{R_I\}$ of nuclei it is sufficient to obtain a set of electronic eigenvalues and eigenfunctions. These eigenvalues, in turn, generate a family of uncoupled potential surfaces on which the nuclear wavefunction can unfold. These uncoupled surfaces can become coupled as a result of taking into account non-adiabatic effects. This type of response by the electrons to the motion of the nuclei is the central theme of the BOA. Neglecting the non-adiabatic effects, which couple the potential surfaces together, and adopting the adiabatic approximation, wherein the electronic wavefunction adjusts itself quasi-statically to the nuclear motion, the motion may be considered only on the ground-state electronic surface. In that case, (2.52) and (2.55) become

$$[K_e + H_I^{ee}(\{\mathbf{r}_i\}) + H_I^{eN}(\{\mathbf{r}_i\},\{\mathbf{R}_I\})]\phi_0^{el}(\{\mathbf{X}_i\},\{\mathbf{R}_I\}) = f_0(\{\mathbf{R}_I\})\phi_0^{el}(\{\mathbf{X}_i\},\{\mathbf{R}_I\})$$

$$[K_N + H_I^{NN}(\{\mathbf{R}_I\}) + f_n(\mathbf{R}_I\})]\phi^{nuc}(\{\mathbf{R}_I\},t) = i\hbar\frac{\partial}{\partial t}\phi^{nuc}(\{\mathbf{R}_I\},t) \text{ ----------2.56}$$

By neglecting the quantum effects in the description of nuclear dynamics, a WKB semi-classical representation for $\phi^{nuc}(\{\mathbf{R}_I\},t)$ can be adopted, and by neglecting terms involving, the classical Hamilton–Jacobi equation is obtained in terms of the classical nuclear Hamiltonian

$$H^{nuc}(\{\mathbf{P}_I\},\{\mathbf{R}_I\}) = \sum_{I=1}^{N} \frac{\mathbf{P}_I^2}{2M_I} + H_I^{NN}(\{\mathbf{R}_I\}) + f_n(\mathbf{R}_I\}). \text{----------2.57}$$

The classical equation for the motion of nuclei on the ground-state surface, defined by the energy

$$E_0(\{\mathbf{R}_I\}) = f_0(\{\mathbf{R}_I\}) + H_I^{NN}(\{\mathbf{R}_I\}), \text{----------2.58}$$

Is given by

$$M_I\ddot{\mathbf{R}}_I = -\nabla_I E_0(\{\mathbf{R}_I\}). \text{----------2.59}$$

To compute the ground-state energy eigenvalue $f_0(\{R_I\})$, the electronic eigenvalue equation (2.56) must be solved. However, an exact solution of this equation is not generally possible, and approximation schemes must be adopted. One such scheme is the use of the density functional theory (DFT), based on the Hohenberg–Kohn theorem [16]. This is an exact theory, formulated in the 1960s, to compute the ground-state of a many-electron system. In this theory, the central notion is that of electron density $n(\{\mathbf{r}_i\})$, and the formalism is constructed in terms of functionals of density. Accurate approximations of these functionals are required, and one approximation of these functionals is the so-called local density approximation (LDA) wherein the properties of an inhomogeneous interacting many-electron system are related to the properties of a homogeneous electron gas. According to the DFT, the total ground-state energy $f_0(\{R_I\})$ of the electrons corresponding to a given configuration $\{R_I\}$ of the nuclei is obtained by minimizing a certain functional, called the Kohn–Sham energy E^{KS} [17], i.e.

$$f_0(\{\mathbf{R}_I\}) = \min_{\phi_0^{el}} \{\langle \phi_0^{el}(\{\mathbf{R}_I\}) \mid H^{el} \mid \phi_0^{el}(\{\mathbf{R}_I\})\rangle\} = \min_{\psi_i} E^{KS}[\{\psi_i\}], \text{----------2.60}$$

where the ψ_i are the Kohn–Sham orbitals and $E^{KS}[\{\psi_i\}]$ is the Kohn–Sham energy functional [17], given by

$$E^{KS}[\{\psi_i\}] = K_s[\{\psi_i\}] + \int d\mathbf{r} H_I^{ext}(\mathbf{r}) n(\mathbf{r}) + \frac{1}{2}\int d\mathbf{r} H_I^{Har} n(\mathbf{r}) + E_{xc}[n] + E_{ions}(\{\mathbf{R}_I\}), \text{----------2.61}$$

where r refers to a single position, and the ψ_i form a set of doubly occupied single-particle states

$$\psi_i(\mathbf{r}), i = 1, 2, ..., \frac{N_e}{2},$$

and each orbital contains an electron with spin up and an electron with spin down, and

$$H_I^{Har}(\mathbf{r}) = \int d\mathbf{r}' \frac{n(\mathbf{r}')}{|\mathbf{r} - \mathbf{r}'|} \text{----------2.62}$$

is the Hartree potential, related to the charge density via Poisson's equation. In terms of the Kohn–Sham orbitals, the charge density is given by

$$n(\mathbf{r}) = \sum_i^{occ} O_i |\psi_i(\mathbf{r})|^2, \text{----------2.63}$$

where $\{O_i\}$ are integer occupation numbers. The Kohn–Sham energy functional (2.63) is minimized by variation, for a fixed number of electrons, with respect to the set of Kohn–Sham orbitals satisfying the orthonormality condition

$$\langle \psi_i \mid \psi_j \rangle = \delta_{ij} \text{----------2.64}$$

leading to the Kohn–Sham equations [17]

$$\left\{-\frac{1}{2}\nabla^2 + H_I^{Har}(\mathbf{r}) + H_I^{xc}[n](\mathbf{r})\right\}\psi_i(\mathbf{r}) = \sum_j \Lambda_{ij}\psi_j(\mathbf{r}), \text{----------2.65}$$

or

$$\left\{-\frac{1}{2}\nabla^2 + H_I^{KS}(\mathbf{r})\right\}\psi_i(\mathbf{r}) = \sum_j \Lambda_{ij}\psi_j(\mathbf{r}), \text{----------2.66}$$

Or

$$H_{eff}^{KS}\psi_i(\mathbf{r}) = \sum_j \Lambda_{ij}\psi_j(\mathbf{r}), \text{----------2.67}$$

where

$$H_I^{xc}[n](\mathbf{r}) = \frac{\delta E_{xc}[n]}{\delta n(\mathbf{r})} \text{----------2.68}$$

is the exchange-correlation potential, and Λ_{ij} are a set of Lagrange multipliers. The Kohn–Sham equations are one-electron equations, and can be expressed in terms of an effective one-electron Hamiltonian H_{eff}^{KS} with H_I^{KS} representing the local potential. The effective one-electron Hamiltonian contains the many-electron effects because of the presence of the exchange-correlation potential, defined in (2.68). The minimization of the Kohn–Sham energy functional (2.61) is performed for each nuclear configuration. Therefore, if the nuclear equation (2.58) is integrated in an MD simulation, then the minimization should be carried out at each MD step and the forces obtained, by using the orbitals thus obtained.

2.4.1 Ab initio Born- Oppenheimer Molecular Dynamics (BOMD)

Contrary to the classical MD where the forces are being derived from classical potentials $H_I(\{r^N\})$ and $\{r^N\}$ represents the spatial coordinates of the individual atoms without the electron dynamics directly considered. Here, the electronic structure is included explicitly in the classical MD simulation. One of the most popular techniques employed to do this is the Born-Oppenheimer MD simulation in which the Kohn-Sham energy functional E^{KS} plays the same role as $H_I\{r^N\}$

$$L^{BO}(\{\mathbf{R}_I\},\{\dot{\mathbf{R}}_I\}) = \sum_{I=1}^{N}\frac{1}{2}M_I\dot{\mathbf{R}}_I^2 - \min E^{KS}[\{\psi_i\};\{\mathbf{R}_I\}] \text{----------2.69}$$

Then the equation of motion of the nuclei is obtained as

$$M_I \ddot{\mathbf{R}}_I = -\nabla_I \left[\min_{\psi_i} E^{KS}[\{\psi_i;\{\mathbf{R}_I\}] \right]$$ ----------2.70

Subject to the condition that

$$\langle \psi_i \mid \psi_j \rangle = \delta_{ij}$$ ----------2.71

The forces needed for the MD simulation are given as

$$F^{KS} = (\mathbf{R}_I) = -\frac{\partial E^{KS}}{\partial \mathbf{R}_I} + \sum_{ij} \Lambda_{ij} \frac{\partial}{\partial \mathbf{R}_I} \langle \psi_i \mid \psi_j \rangle.$$ ----------2.72

[1]

CHAPTER THREE

3.0.0 METHODOLOGY

For the classical molecular Dynamics, the following procedures are taken.

Using the NVT ensemble for MD, the number of atoms, temperature and volume are kept constant at every instant. For these, the Nose-Hoover thermostat is used to rescale the temperature of the system to 800K.

The catalyst used is Fe nanoparticles with core atoms at fcc position. For this work, no substrate is incorporated as a base for the nanoparticle but the growth is still expected to go on well since the substrate only defines the type of growth as to whether it will be either a tip growth or a base growth.

The simulation is carried out using Large Atom/Molecule Massively Parallel Simulator (LAMMPS) code under periodic boundary condition. There were 200 carbon atoms deposited on the Fe nanoparticles which serve as the catalyst each at the rate varying from 20-30 ps per atom.

The modified embedded atom potential method (MEAM) potential [15] was used as the interaction potential that existed between the C-C, C-Fe and the Fe-Fe.

The procedure for the ab initio simulation goes thus;

The atomic positions for the fcc iron and the carbon atoms arranged on it are determined and placed in an 'scf' calculation input script. It is then visualized with XCRYSDEN [13]

The equilibrium lattice constant and bulk modulus are determined for a cutoff of 60 Ry and 4x4x4 k-point grid. The experimental lattice constants for iron and carbon used are 6.7463bohr and 5.4235 bohr respectively. The resulting curve of E (total) against lattice parameter is fitted using the Murnaghan equation of state. Here, the code used is the QUANTUM ESPRESO [19]. PBESOL functional [21] is used which is obtained by changing some parameters in the Pedrew-

Burke-Enzerhof (PBE) [20] functional and it is designed for solids. The pseudopotentials are ultrasoft type having eight electrons ($3d^6 4s^2$) and six electrons ($1s^2 2s^2 2p^2$) for Fe and C, respectively.

The one electron wavefunction can be expanded using PWSCF code in basis functions that are plane waves. The plane waves are chosen such that its periodicity is compatible with the periodic boundary condition of the simulation cell. Therefore, the plane waves used extends to a cutoff value which makes the expansion finite during calculations. The units of the cutoff are in Rydberg (Ry.). Using PWSCF code, the energy of carbon and iron as a function of ecutwfc is determined by varying the cutoff from 60 to 200 Ry at interval of 5 while every other variables like the lattice parameter and k-points are kept constant. The required cutoff energy for a convergence of the energy to within 1 mRy is to be determined.

For carbon (fcc) which crystallizes to a diamond structure, the accuracy of 1 mRy per atom corresponds to a cutoff of 75 Ry. Similarly for iron (bcc), the cutoff corresponding to 1mRy per atom is 80 Ry. Therefore, a cutoff of 80 Ry is suitable for the calculation.

The corresponding plots are displayed below.

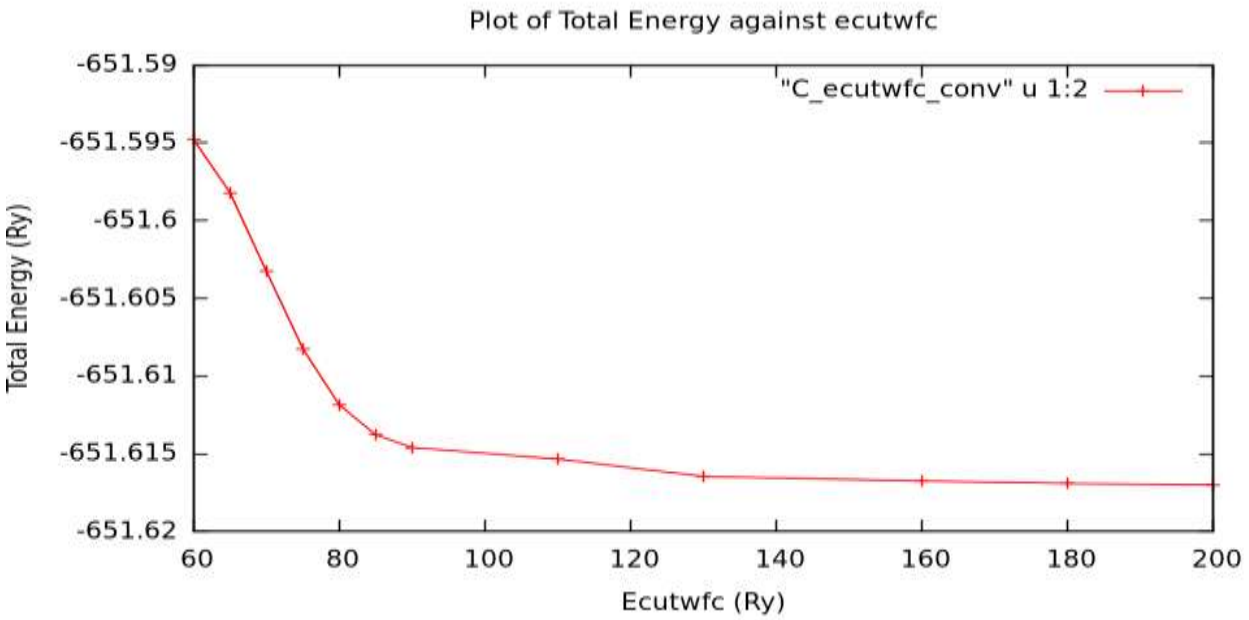

Fig. 4.4 A plot of total energy against the ecutwfc for carbon.

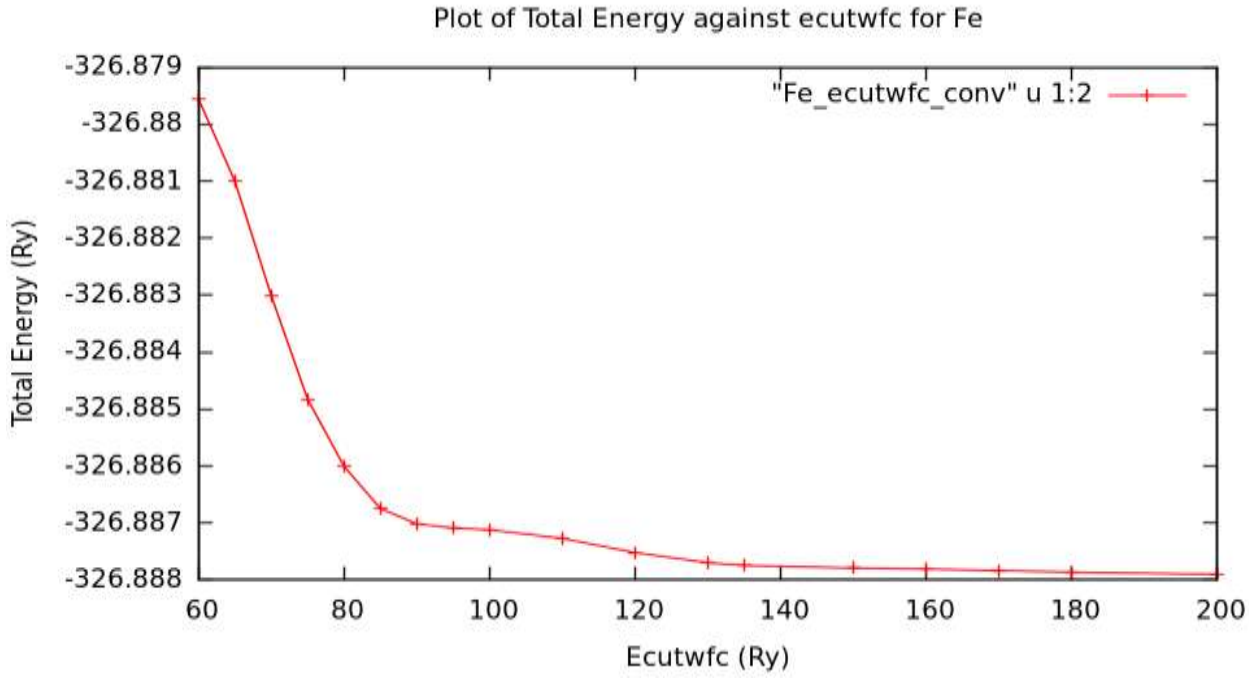

Fig 4.5 A plot of total energy against the ecutwfc for iron.

The energy decreases monotonically with increasing cutoff being a direct consequence of the variational principle which predicts the over estimation of the ground state for a set of basis that

is not infinite. In this case, large number of cutoff energy (i.e. 200 Ry) is required so as to get to the ground state energy approximately.

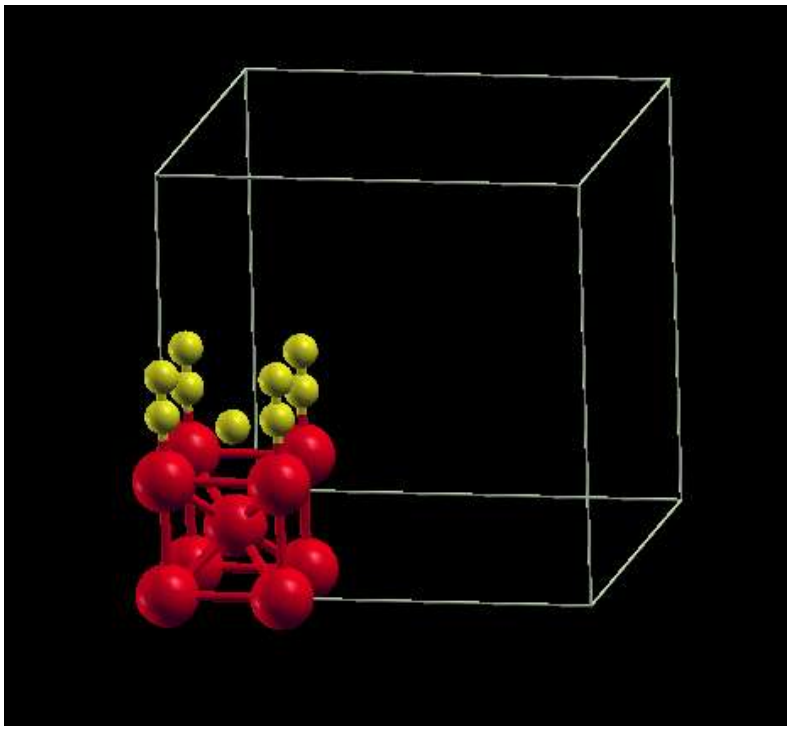

Fig. 4.6 The XCRYSDEN [13] was used to display the figure.

A ‘vc-relax’ (variable cell relaxation) calculation is then carried out with nstep of 50 for achieving an optimization of the geometry.

CHAPTER FOUR

4.0.0 RESULTS

4.1.0 Classical MD Simulation

The following the results were obtained from the simulation using the LAMMPS code.

The simulation was carried out at different deposition rates. For a deposition of 1 C randomly at every 20ps near the nanocluster surface, some of the carbon atoms were observed to be floating in air, this is rather too fast and leads to inability to anneal the structure formed before adding another carbon atom. Thus a deformed geometry observed.

For a deposition time of between 25-30ps per 1 C atom, most of the carbon came together to form a tube- like structure on the Fe nanocluster.

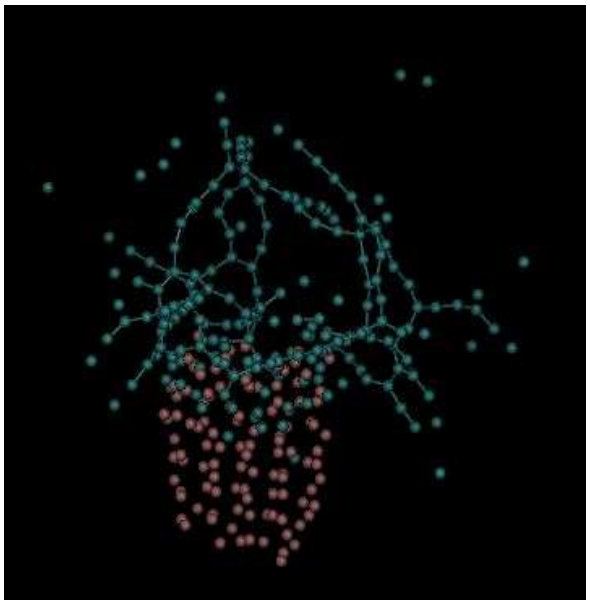

Fig. 4.1 1 C added randomly every 20ps near the Fe nanocluster surface.

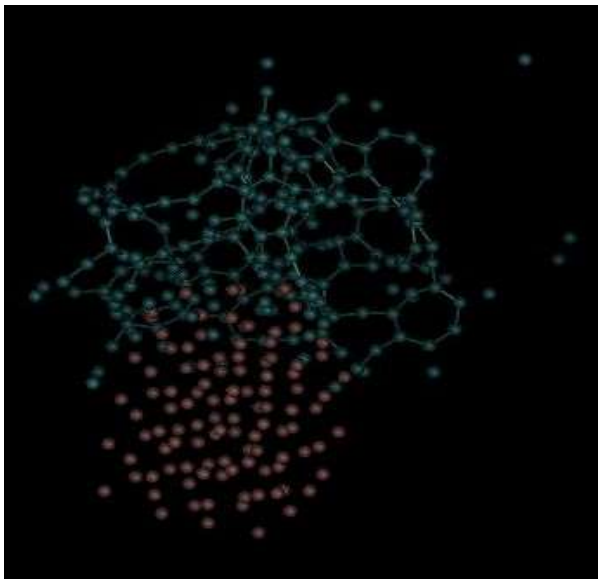

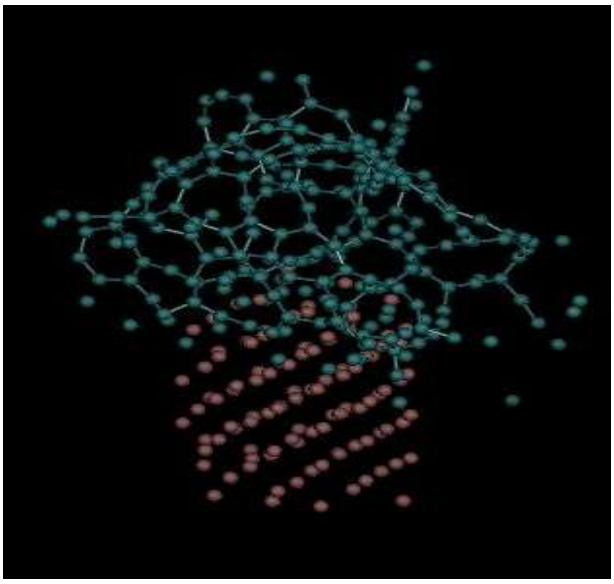

Fig. 4.2a 1 C added randomly every 25ps Fig 4.2b 1 C added randomly every 30ps

A closer study at the early stage of the process reveals the gradual formation of the cap and revealing the sp2 hybridization.

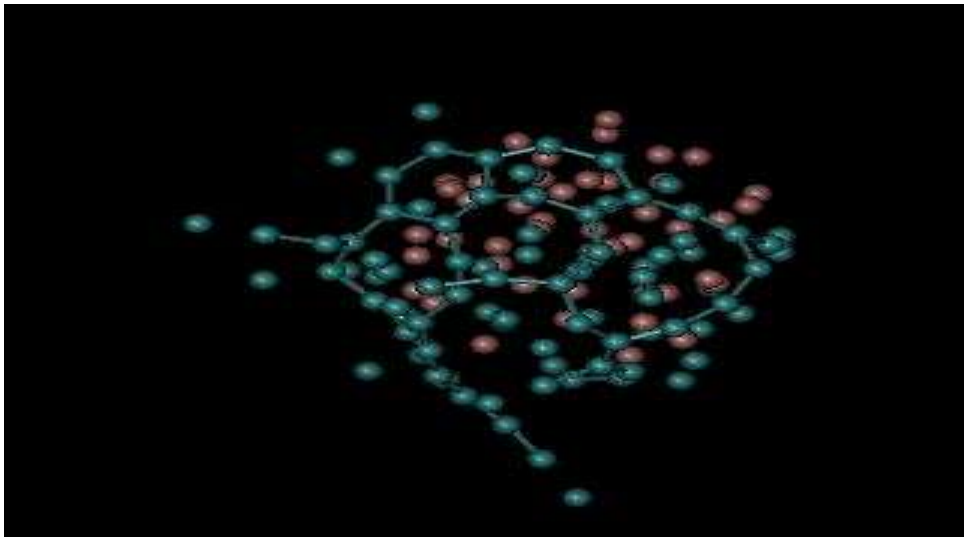

Fig. 4.3 Top view of nanotube cap formation at the early stage of 40secs.

4.2.0 AB INITIO OPTIMIZATION

In our quest to understand the growth processes leading to CNTs, we optimized a small cluster of carbon atoms on iron atoms (catalyst). We started with nine carbon atoms placed randomly atop a small cluster of iron atoms in the BCC configuration (see Fig. 4.6 below).

The PBESOL density functional by GI Csonka et. al. [21] is used with ultrasoft pseudopotentials having eight electrons ($3d^6 4s^2$) and six electrons ($1s^2 2s^2 2p^2$) for Fe and C, respectively.

4.2.1 DETERMINATION OF THE EQUILLIBRUM LATTICE CONSTANT AND BULK MODULUS

First, to ascertain the accuracy of the functional and the pseudopotentials which we plan to use for the Fe-C system, we computed the equilibrium lattice constants and bulk moduli for bulk iron (FCC) and bulk carbon (Diamond). For carbon and iron separately, and using an energy cutoff of 60 Ry and a symmetric K-point grid of 4x4x4, the lattice constants are calculated by varying the lattice constants for various values around the known experimental value. The results obtained are presented with column 1 being the lattice constant and column 2 their corresponding total energy. Finally, the result is then fitted to the Murnaghan equation of state [14] to obtain the lattice parameter (a_0) and the equilibrium bulk modulus (K_0) at the minimum position.

The following are obtained.

4.2.2 RESULTS OF THE MURNAGHAN FIT FOR CARBON

Table 4.1 Showing the Murnaghan fit for Carbon Calculations.

equation of state: murnaghan. chisq = 0.4993D-04 a0 = 6.75 a.u., k0 = 3841 kbar, dk0 = 3.31 d2k0 = 0.000 emin = -36.22400 a0 = 3.575 Ang, k0 = 384.1 GPa, V0 = 77.055 (a.u.)^3, V0 = 11.418 A^3					
Lat.par (a.u.)	E-calc (Ry)	E_fit (Ry)	E_diff (Ry)	Pressure (GPa)	Enthlpy (Ry)
8.246	-35.92983	-35.92293	-0.00690	-100.08	-36.88363
7.746	-36.06616	-36.07637	0.01021	-86.29	-36.74782
7.246	-36.17821	-36.18283	0.00462	-58.28	-36.55509
6.746	-36.23087	-36.22398	-0.00689	1.46	-36.22324
6.246	-36.16922	-36.16173	-0.00749	136.35	-35.60446
5.746	-35.90564	-35.91396	0.00832	461.70	-34.41677
5.246	-35.29634	-35.29447	-0.00186	1309.90	-32.08169

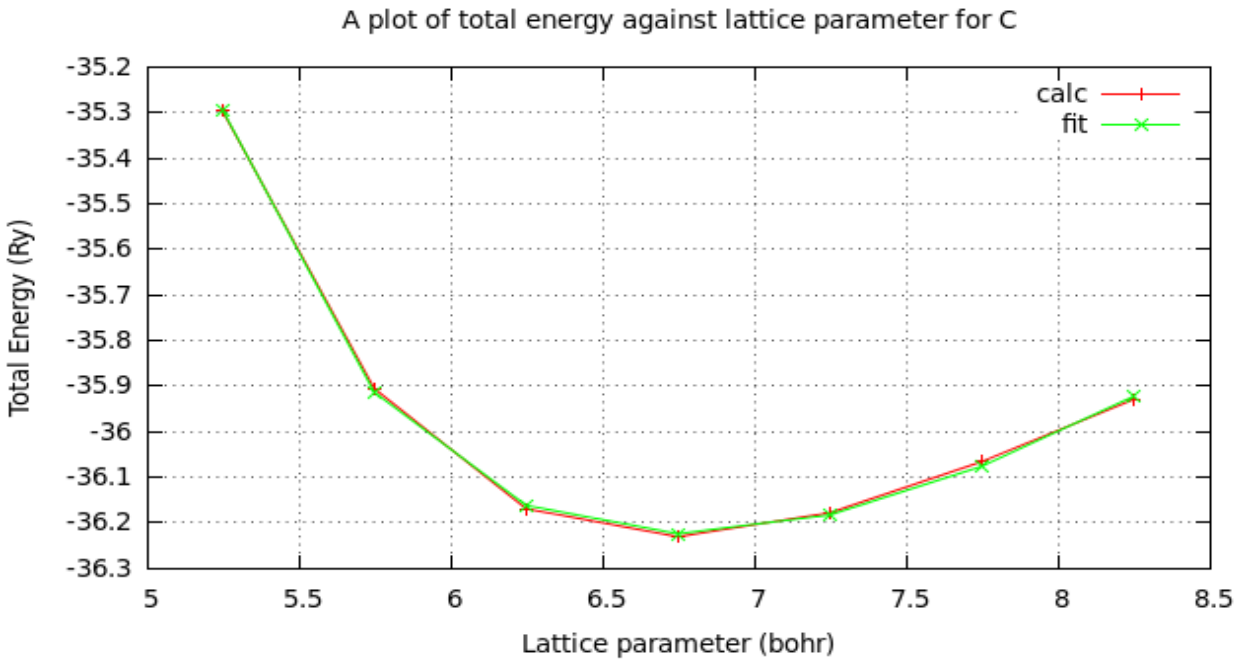

Fig. 4.7

4.2.3 RESULTS OF THE MURNAGHAN FIT FOR IRON

Table 4.2 Showing the Murnaghan fit for Iron Calculations.

equation of state: murnaghan. chisq = 0.1540D-03 a0 = 5.26 a.u., k0 = 2207 kbar, dk0 = 3.74 d2k0 = 0.000 emin = -326.87384 a0 = 2.781 Ang, k0 = 220.7 GPa, V0 = 72.599 (a.u.)^3, V0 = 10.758 A^3					
Lat.par (a.u.)	E-calc (Ry)	E_fit (Ry)	E_diff (Ry)	Pressure (GPa)	Enthlpy (Ry)
6.717	-326.66596	-326.64937	-0.01659	-55.24	-327.23495
6.217	-326.75304	-326.76267	0.00962	-50.04	-327.16172
5.717	-326.83514	-326.84332	0.00818	-36.04	-327.06400
5.217	-326.88029	-326.87356	-0.00673	5.14	-326.85549
4.717	-326.81421	-326.80218	-0.01203	139.69	-326.31591
4.217	-326.45010	-326.47110	0.02100	639.70	-324.81958
3.717	-325.33752	-325.33407	-0.00345	2821.17	-320.41317

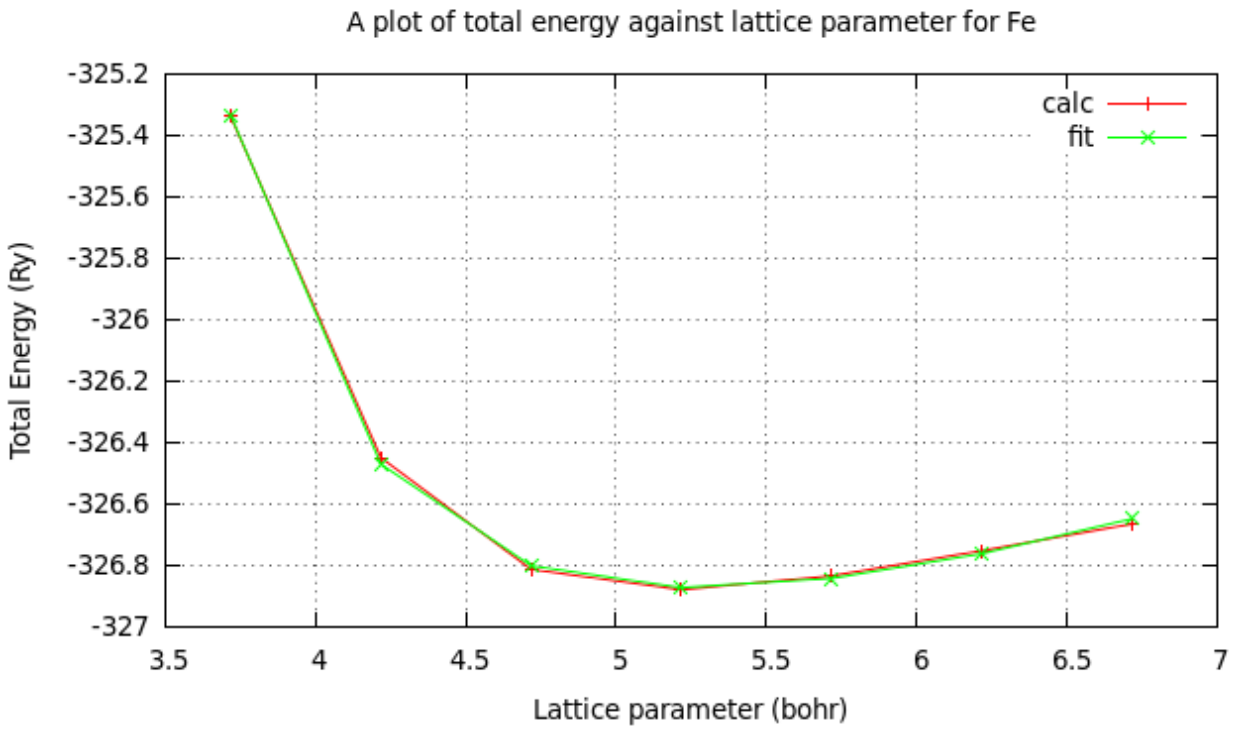

Fig. 4.8

Table 4.3 Comparism of the experimental with the obtained values of a_0 and K_0

	Experiment		Obtained	
Element	Lattice constant a_0 (bohr)	Bulk modulus K_0 (GPa)	Lattice constant a_0 (bohr)	Bulk modulus K_0 (GPa)
C	6.7403(b)	442(b)	6.75	384.1
Fe	5.4235(a)	168.3(a)	5.26	220.7

a-C.Kittel, introduction to solid state Physics, 7th ed. (Wiley, New York,1996)
b-Javier Junquera etal. Phys. Rev.B64, 235111(2001).

4.2.4 VARIABLE CELL CALCULATION

A variable cell calculation is often performed to achieve a geometry optimization of a given system for which the lattice parameters and atomic positions are not known exactly. It might be difficult to find a ground state structure with a large lattice constant if the supercell used is very small since the atoms are brought very close to one another. The usual thing to do is to perform a variable cell calculation which allows the optimization of both the size and shape of the supercell along with the atomic positions. Therefore, a 'vc-relax' (variable cell relaxation) calculation is carried out. This is done so as to achieve a geometric optimization with variable unit cell coordinates.

Below is a view of the atomic positions obtained from the ‘vc-relax’ calculations.

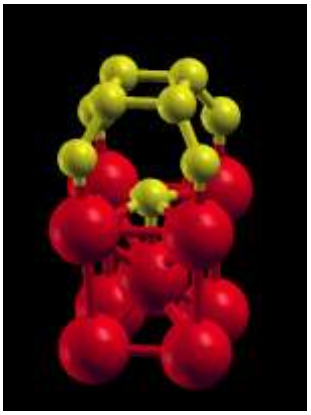

Fig. 4.9 A view of the new arrangement of the carbon after a ‘vc-relax’ calculation. The cap formed reveals the origin of an armchair CNT.

4.3.0 DISCUSSION

From out of classical MD simulations, the structures formed are not of the right CNT geometry and the cap not properly formed due to defects in the structure. Many factors could have been responsible for these some of which are; the operating temperature at which the nucleation and growth is carried out, the non- equilibrium conditions, assumptions made during the MD simulations and the inability to simulate correctly the thermodynamic conditions that favor the nucleation growth among others. From observation, CNT growth process is a complicated mechanism with unpredictable and disordered dynamics[9]. This disordered dynamics most likely gives birth to the defects in the CNT during the growth process.

The result obtained is however in good coherence with the work of Alister *et. al.* [9] which established that SWNT growth is an '*inherently defective process*'. They further re-iterated that defects in polyyne chains formations, non hexagonal ring structures and the imbedded vacancies in the sp^2-hybridized carbon network are all inherently peculiar to the growth process of SWNT which is no different in the present work. Crucial to the observation of this work is the fact that the cap formation on the catalyst reveals a defect in the ring. These defects are thus being propagated through the walls of the tube during the process. One can therefore infer that the difficulty in the selection process of a specific chirality is partly due to these facts.

For the ab- initio simulation, the lattice constant and the bulk modulus of the C and Fe obtained is in good comparism with experimental values. After the 'vc-relax' calculation, the viewing of the new atomic positions reveals the formation of a CNT cap.

4.4.0 CONCLUSION AND RECOMMENDATION

This work reveals the defects resulting from the nucleation and growth of SWCNT and how they are propagated throughout the structure. It discovers that the chirality alteration and the variation in the physical properties of the material were due to the defects incurred in the growth process. It further supports the results of Alister *et. al.*[9] about the non-linear dynamics of SWNT process. The results from the ab initio simulation are promising but not concluded yet.

I therefore recommend that further work be carried out based on the proper understanding of the chemical kinetics of the growth process. Also the QM simulation aspect of this work should be completed and relevant comparism be made and conclusions drawn out.

4.5.0 APPENDIX

4.5.1 LAMMPS Codes for the Classical Molecular Dynamics

```
# michael's thesis
# ------------------------ INITIALIZATION ----------------------
clear
units           metal
dimension       3
boundary        p       p       p
atom_style      atomic


# ----------------------- ATOM DEFINITION -----------------------

lattice         sc  3.56 orient x 1 0 0 orient y 0 1 0 orient z 0 0 1
region          upper1 block  -1.0  1.0  -1.0  1.0  5  5  units lattice
region          upper2 block  -1.0  1.0  -1.0  1.0  6  6  units lattice
lattice         fcc  2.87  orient x 1 0 0 orient y 0 1 0 orient z 0 0 1
region          lower block -1.0  1.0  -1.0  1.0  0  4.0 units lattice
region          big block    -7.5 7.5  -7.5  7.5 0 25  units lattice
region          whole union 2 lower big
create_box      2 whole
lattice         sc  2.87  orient x 1 0 0 orient y 0 1 0 orient z 0 0 1
create_atoms    1 region lower
lattice         fcc 3.56 orient x 1 0 0 orient y 0 1 0 orient z 0 0 1
#create_atoms 2 region upper1
group Carbon  region upper1

# ------------------------ FORCE FIELDS -----------------------

pair_style meam
pair_coeff * * FeC.library.meam  Fe  C  FeC.meam  Fe  C


#---------------------------Settings----------------------------
compute csym all centro/atom fcc
compute eng all pe/atom
compute eatoms all reduce sum c_eng
compute strs all stress/atom

#----------------------Run Minimization-------------------------
#fix 1 all box/relax  iso  0.0  vmax  0.001
dump 1 all atom 200 dumpTemp.lammpstrj
```

```
thermo 100

reset_timestep 0
thermo 100
neighbor 0.3 bin
timestep 0.25e-3
velocity all create 800 123 dist gaussian
fix 1 all nvt temp 800.0  800.0 0.01  tchain 4

run 800000

fix 2 Carbon deposit 200 2 100 1145788 region upper1 global 5.0  5.0   near 0.25  target 0.0  0.0
6.0
fix 1 all nvt temp 800.0  800.0 0.01  tchain 4

run 800000

########################################
# SIMULATION DONE
print "All done"
```

4.5.2 Quantum Espresso input for the geometry and variable-cell optimization

```
&control
 calculation='vc-relax'
   restart_mode='from_scratch'
   prefix='FeC',
   pseudo_dir = './',
   outdir='./',
   nstep=50,
   dt=20,


 /
 &system
   ibrav=  1, celldm(1) = 20.00, nat= 18, ntyp= 2,
   ecutwfc= 80.0,
   occupations= 'smearing', smearing= 'marzari-vanderbilt'
   ecutrho= 960, starting_magnetization (1)=0.7,
   degauss= 0.05, nbnd=120

 /
 &electrons
!conv_thr = 1.0e-8
mixing_beta = 0.7
mixing_mode = 'local-TF'
```

```
diagonalization='cg'
 /

 &ions
 ion_dynamics='damp',
 /
&cell
cell_dynamics = 'damp-w',
wmass = 0.0001,

 /

ATOMIC_SPECIES
 Fe  55.847 Fe.pbesol-spn-kjpaw_psl.0.2.1.UPF
 C   12.00  C.pbesol-n-kjpaw_psl.0.1.UPF


ATOMIC_POSITIONS (angstrom)
 Fe 0.00 0.00 0.00
 Fe 2.87 0.00 0.00
 Fe 2.87 2.87 0.00
 Fe 2.87 0.00 2.87
 Fe 2.87 2.87 2.87
 Fe 0.00 2.87 0.00
 Fe 0.00 2.87 2.87
 Fe 0.00 0.00 2.87
 Fe 1.435 1.435 1.435
 C 0.00 0.00 4.50
 C 0.00 2.87 4.50
 C 2.87 2.87 4.50
 C 2.87 0.00 4.50
 C 1.435 1.435 3.92
 C 0.00 0.00 5.50
 C 0.00 2.87 5.50
 C 2.87 2.87 5.50
 C 2.87 0.00 5.50

K_POINTS (automatic)
4  4  4  1  1  1
```

4.5.0 REFERENCES

[1] I. H. RAFII - TABAR (Shahid Beheshti University of Medical Sciences and the Institute for Research in Fundamental Sciences, *COMPUTATIONAL PHYSICS OF CARBON NANOTUBES*. CAMBRIDGE UNIVERSITY PRESS, 2008.

[2] J.-Y. Raty, F. Gygi, and G. Galli, "Growth of Carbon Nanotubes on Metal Nanoparticles: A Microscopic Mechanism from Ab Initio Molecular Dynamics Simulations," *Physical Review Letters*, vol. 95, no. 9, p. 096103, Aug. 2005.

[3] S. Reich, L. Li, and J. Robertson, "Control the chirality of carbon nanotubes by epitaxial growth," *Chemical Physics Letters*, vol. 421, no. 4–6, pp. 469–472, Apr. 2006.

[4] Y. Liu, A. Dobrinsky, and B. I. Yakobson, "Graphene Edge from Armchair to Zigzag: The Origins of Nanotube Chirality?," *Physical Review Letters*, vol. 105, no. 23, p. 235502, Dec. 2010.

[5] M. Meyyappan, L. Delzeit, A. Cassell, and D. Hash, "Carbon nanotube growth by PECVD: a review," *Plasma Sources Science and Technology*, vol. 12, no. 2, pp. 205–216, May 2003.

[6] A. F. Nobuhito Inami, Mohd Ambri Mohamed, Eiji Shikoh, "Synthesis-condition dependence of carbon nanotube growth by alcohol catalytic chemical vapor deposition method." ELSEVIER, Science and Technology of Advanced Materials 8(2007). 292-295.

[7] S. Banerjee, S. Naha, and I. K. Puri, "Molecular simulation of the carbon nanotube growth mode during catalytic synthesis," *Applied Physics Letters*, vol. 92, no. 233121, pp. 1–3, 2008.

[8] N. 668-8502 J. Mukul Kumar (Department of materials Science & Engineering, Meijo University, "Carbon Nanotube Synthesis and Growth Mechanism," in *Nanotechnology and Nanomaterials*, D. Y. Siva, Ed. .

[9] S. I. and K. M. Alister J. page, Ying Wang, K.R.S. Chandrakumar, "Mechanisms of Single-walled Carbon Nanotube Nucleation, Growth and Chirality-Control: Insight from QM/MD Simulations," pp. 1–39, 2011.

[10] G. D. , M. D. and R SAITO, *Physical Properties of Carbon Nanotubes*. Imperial College Press.1st ed. 1998

[11] C.Kittel, introduction to solid state Physics, 7th ed. (Wiley, New York,1996)

[12] Javier Junquera etal. Phys. Rev.B64, 235111(2001).

[13] A. Kokalj, Comp. Mater. Sci., Vol. 28, p. 155, 2003.

[14] F.D Murnaghan, Proc. Nat.Acad.Sci 30,244(1944)

[15] Byeong-Joo Lee "A modified embedded-atom method interatomic potential for the Fe–C system" Acta Materialia, vol. 54, no. 3, pp.701-711, Nov. 2005

[16] R. G. Parr andW. Yang, Density Functional Theory of Atoms and Molecules, (Oxford: Oxford University Press, 1989).

[17] J. Hutter, Introduction to ab Initio Molecular Dynamics, Lecture Notes (University of Zürich, 2002).

[18] H. Dai, Surf. Sci., 500 (2002), 218.

[19] P. Giannozzi *et. al*., J. Phys.:Condens. Matter 21 395502 (2009)

[20] JP Perdew, K Burke, M Ernzerhof - Physical review letters, 1996 - APS

[21] GI Csonka, A Ruzsinszky, JP Perdew et. al. - J. Chem. Theory Comput.2008,4,888–891, 2008 - ACS Publications